Optics Communications 284 (2011) 3772–3784

Contents lists available at ScienceDirect

Optics Communications

journal homepage: www.elsevier.com/locate/optcom

Invited Paper

Linear self-referenced complex-field characterization of fast optical signals using photonic differentiation

José Azaña *, Yongwoo Park [1], Fangxin Li [2]

Institut National de la Recherche Scientifique – Energie, Matériaux et Télécommunications (INRS-EMT), 1650, Boul. Lionel-Boulet, Varennes, Québec, Canada J3X 1S2

ARTICLE INFO

Article history:
Received 15 December 2010
Received in revised form 25 February 2011
Accepted 27 February 2011
Available online 16 March 2011

Keywords:
Ultrafast optical signal characterization
Ultrashort pulse measurements
Phase reconstruction
Linear optical signal processing
Photonic differentiation
Fiber-optics technologies
Optical telecommunications

ABSTRACT

This paper reviews recent work on a new group of linear and self-referenced techniques for full (amplitude and phase) characterization of fast optical signals based upon the concept of photonic differentiation, generally referred to as 'phase reconstruction using optical ultrafast differentiation' (PROUD). These techniques are particularly well adapted for applications in the context of fiber-optics telecommunications. PROUD methods can be implemented using simple and practical optical fiber-based setups and they rely on a direct, non-iterative phase recovery numerical algorithm. They can be used over a very wide range of pulse time durations, from the sub-picosecond to the nanosecond regime, and they can provide measurements in a single shot and in real time with power sensitivities down to the microwatt level. Previously reported PROUD methods are treated here under a unified, single framework, facilitating their analysis and comparison.

1. Introduction

Many applications in a wide range of scientific and technical fields, including physics, chemistry, microwave and optical engineering, are based on the use of fast optical signals (e.g. ultra-short light pulses) [1]. Accurate measurement and full characterization of such optical signals is thus an essential task [2–7]. This topic has attracted a considerable attention from the relevant technical communities for many years and this is still today a very active area of research. Some excellent review papers on this area have recently appeared in the specialized literature [4–7]. The reader is addressed to these previous papers for a detailed account on historical developments and a comprehensive overview of available methods and technologies for light pulse characterization.

A large variety of optical pulse characterization methods have been developed over the years. Each different method and technology offers a different set of performance specifications and is thus particularly suitable for a specific range of applications. The focus of this work is on techniques adapted to the problem of full characterization of low-intensity, fast optical signals, such as those to be found in fiber-optics telecommunication systems [5,7]. In an optical communication link [8], the information is encoded on the electric field of an optical source in various ways, e.g. by amplitude modulation, and/or phase modulation. In all cases, the encoded optical information must propagate through a transmission medium (optical fiber) and a variety of photonics and opto-electronic components, such as filters, multiplexers, amplifiers, temporal modulators etc. Each affects the electric field of the transmitted signal by multiple physical effects, including dispersion, nonlinearities, amplified spontaneous emission, filtering etc. For a full characterization of these impairments, complete information on the evolution of the time-domain and/or spectral-domain amplitude and phase profiles of the signals under test is necessary. The ability to measure optical phase information is increasingly important due to the ongoing adoption of different phase-shift-key modulation formats in fiber-optics telecommunication systems [9].

Conventional square-law photo-detectors can be used to partly characterize optical signals with a spectral bandwidth <50 GHz. For instance, this is useful for per-channel data stream measurement in telecommunication systems based on dense wavelength-division-multiplexing (DWDM) formats. However, photo-detection provides information only on the temporal intensity profile of the signals under test. Interferometer-based schemes combined with balanced photo-detection, so-called 'coherent receivers' [10], can extend these capabilities to provide phase information of the optical signals (e.g. for digital data decoding) but these strategies are typically suitable for application only on a specific modulation format and at a prescribed bit rate. Whereas techniques have been demonstrated to extend the use of temporal coherent receivers for full recovery of arbitrary phase variations [11], they require the use of a precisely synchronized optical

* Corresponding author.
E-mail address: azana@emt.inrs.ca (J. Azaña).
[1] Present address: Automated Precision Inc., 15000 Johns Hopkins Dr., Rockville, MD, USA.
[2] Present address: CUDOS, School of Physics, University of Sydney, New South Wales 2006, Australia.

0030-4018/$ – see front matter © 2011 Elsevier B.V. All rights reserved.
doi:10.1016/j.optcom.2011.02.079

reference. Moreover, conventional photo-detection cannot provide the temporal resolution (bandwidth) that is required to capture even the temporal intensity profile of the signals to be found in communication links operating at serial data rates beyond ~50 Gb/s, e.g. links based on optical-time-division-multiplexing (OTDM). Pulse durations in the picosecond range or shorter are employed in these systems.

There are several well-established ('classical') methods for full characterization of optical pulse waveforms with time features down to the femtosecond range, including FROG (Frequency-Resolved Optical Gating) [3,12], SPIDER (Spectral Phase Interferometry for Direct Electric-Field Reconstruction) [13], and any of their multiple variants [6]. These techniques have been traditionally implemented by use of optical non-linearities in a variety of material and/or waveguide technologies. Over the years, these methods have been adapted to operate on a broader range of pulse time durations, frequency bandwidths and energies. However, most of the presently available non-linear pulse characterization techniques cannot easily satisfy the requirements for application in optical telecommunications [7,8]. Ideally, an optical signal characterization method suitable for fiber-optics communications should be able to process a wide range of pulse durations, from the sub-picosecond to the nanosecond regimes. The method should also be sensitive enough to characterize optical signals with sub-milliwatt average powers. Moreover, in an optical network, sources are data encoded and the randomness of the data (non-periodic signals) may preclude averaging, thus requiring single-shot sampling capabilities. Measurement techniques providing fast update rates are also highly desired so that to be able to monitor the optical signals in real time. Finally, self-referenced techniques are preferred given that a precisely synchronized/correlated optical reference, e.g. a local oscillator, may not be always available; the need for a reference, in the measurement setup (e.g. as in reference-based interferometry [11,14–16]) also introduces a higher level of complexity in the measurement platform. Obviously, the development of optical pulse measurement methods capable of providing this set of stringent performance specifications is of interest for applications beyond the field of optical telecommunications, e.g. for pulse-based sensing and imaging systems [1] and for signal monitoring in linear optical computing and information-processing circuits [17].

In view of all these needs, a significant research effort has been devoted towards the development of *self-referenced* pulse characterization techniques based on *linear optics* [5,18–38]. Recent demonstrations include both linear implementations of concepts previously proved with non-linear processes (e.g. spectrography [18,19] and spectral self-interferometry [20,21]) and fundamentally new linear-optics pulse measurement schemes [22–38]. As compared with more conventional non-linear optics techniques, linear-optics methods offer an increased sensitivity and they can be implemented in very simple and practical (e.g. fiber-based) platforms. In this paper, we review a recent body of work on a new group of linear and self-referenced techniques for full characterization and monitoring of fast optical signals based upon the concept of *photonic differentiation*, generally referred to as 'phase reconstruction using optical ultrafast differentiation' (PROUD) [33–38]. These methods are particularly well adapted to the problem of signal characterization in the context of optical telecommunications. PROUD techniques can be used for full characterization of optical signals, including continuous-time data streams, over a very wide range of pulse time durations, from ~100 fs to well in the nanosecond regime [33–35]; they can provide measurements in a single-shot and in a real-time with power sensitivities down to the microwatt level [36–38]. Real-time operation is in part enabled by the fact that the PROUD methods rely on a simple, non-iterative phase recovery numerical algorithm (simple analytic equation). The PROUD methods can be implemented using off-the-shelf fiber-optics and RF components and the resulting setups are thus very simple and fully compatible with fiber systems.

In its most basic implementation, time-domain PROUD [33,35], the temporal phase profile of an optical signal can be recovered from two time-domain intensity measurements, namely the intensity profile of the signal under test and that of the resulting signal following photonic temporal differentiation. A photonic temporal differentiator is a linear optical filter capable of 'calculating' the time derivative of the temporal complex envelope of an incoming optical signal [17,39]. This functionality, essentially a photonic frequency discriminator, can be practically implemented by means of a variety of fiber-optics technologies, including a uniform long-period fiber grating (LPFG) [40], an apodized, chirped fiber Bragg grating [41], or a fiber-optics Mach–Zehnder interferometer [42]. Photonic temporal differentiators can be also implemented using integrated-waveguide filters [39,43] and bulk-optics interferometers [44]. Using time-domain PROUD, the capabilities of any available temporal intensity measurement setup, e.g. a conventional photo-detector attached to a sampling or real-time scope, can be easily upgraded to characterize the signal temporal phase profile. Low-power optical pulse waveforms with durations ranging from a few picoseconds to a few nanoseconds, and with bandwidths from the sub-GHz range to the terahertz range, can be accurately characterized using time-domain PROUD (with conventional photo-detection) combined with dispersion-induced time stretching [35]. By incorporating a balanced/differential photonic differentiation and photo-detection scheme, single-shot and real-time characterization of the instantaneous frequency and phase profiles of low-power (microwatt) continuous-time optical data streams with frequency bandwidths >10 GHz has been successfully demonstrated [36]. Whereas several self-referenced techniques have been specifically developed for instantaneous frequency characterization of telecommunication GHz-bandwidth optical signals, including methods based upon the use of photonic frequency-discriminator filters [27–31], they rarely offer single-shot and real-time capabilities, as desired for practical monitoring applications. Moreover, time-domain balanced PROUD can be easily extended for simultaneous full characterization of many multi-wavelength (e.g. WDM) signals [37].

A frequency-counterpart of the time-domain PROUD concept can be realized by processing the signal under test with a photonic *frequency* differentiator [34]. This is a linear device capable of calculating the frequency derivative of the signal's field spectrum and it can be easily implemented by use of a conventional electro-optic (EO) intensity modulator driven by an electrical sinusoid. Using this approach, the signal spectral phase profile, leading to a full characterization of the optical signal, can be recovered from measurements of the energy spectra of the signal and of its frequency derivative. In contrast to a variety of linear pulse characterization methods based on EO phase modulation [20,21,32], the use of intensity modulation facilitates implementation of the measurements since monitoring of the temporal modulation process is greatly simplified. This method is suitable for measuring the complex-field profile of low-power optical pulses with durations from ~100 fs to ~15 ps [34], thus being perfectly complementary to time-domain PROUD. Single-shot and real-time full characterization of low-power (microwatt) picosecond and sub-picosecond waveforms have been recently demonstrated [38] using an advanced spectral-domain PROUD setup based on the balanced differentiation concept combined with dispersion-induced time stretching. Very few linear, self-referenced picosecond pulse characterization methods can provide single-shot and real-time capabilities [5].

In this paper, all the PROUD schemes developed up to date are presented in a fully consistent fashion, under a single, unified framework. This facilitates the comparison between the different methods, including a clear definition of the capabilities and limitations of each scheme in relationship with the rest of the PROUD techniques. The remainder of this paper is organized as follows. Section 2 is devoted to the basic time-domain PROUD technique, including its operation principle (2.1), a brief discussion of its main performance

trade-offs (2.2), and an experimental application example (2.3). The same organization is used in Section 3 to discuss the basic spectral-domain PROUD concept. Section 4 focuses on the balanced PROUD concept for single-shot and real-time optical signal characterization applied to both the time-domain and spectral-domain techniques. The general concept is introduced in Section 4.1 and application examples are subsequently discussed for the time-domain technique (4.2, with an example of multi-wavelength signal characterization) and the spectral-domain (4.3) technique. Finally, some general conclusions are drawn in Section 5.

2. Time-domain phase reconstruction using optical ultrafast differentiation (PROUD)

2.1. Operation principle of time-domain PROUD

Fig. 1 illustrates the principle of operation of time-domain PROUD. The signal under test is supposed to be spectrally centered at the optical radial frequency ω_0, having a time-domain complex envelope defined by $x(t)=|x(t)|\exp(j\phi(t))$, where $|x(t)|^2$ and $\phi(t)$ are the signal's time-domain intensity and phase profiles, respectively. The field frequency spectrum of the signal envelope can be calculated as the Fourier transform (FT) of $x(t)$; in particular $X(\omega)=FT\{x(t)\}=|X(\omega)|\exp(j\Phi(\omega))$, where $|X(\omega)|^2$ and $\Phi(\omega)$ are the spectral energy density and spectral phase profile of the signal, respectively. In this notation, ω is the base-band radial frequency, i.e. $\omega=\omega_{opt}-\omega_0$ with ω_{opt} being the optical radial frequency variable. Time-domain PROUD [33] is based on extracting the signal temporal phase profile from two temporal intensity waveform measurements, namely the time-domain intensity profiles of the signal under test and of the signal after propagation through a frequency-shifted temporal photonic differentiator. Such a device is a linear time-invariant optical filter characterized by a spectral transfer function having a linear-amplitude variation, $D(\omega)=A(\omega+\Delta\omega)$, where A is the (positive or negative) slope of the linear spectral amplitude variation and $\Delta\omega$ is the (positive) frequency shift between the signal's central frequency and the resonance frequency of the differentiator. Notice that by 'resonance frequency' of the differentiator we refer to the frequency at which its spectral transfer function reaches zero. It is also important to note that the filtering transfer function defined above, with $\Delta\omega$ being a positive number, corresponds to the case when the signal's carrier frequency is higher than the filter's resonance frequency. A linear spectral-amplitude filter is usually referred to as a 'frequency discriminator'. The name used here to denote this optical filter is associated with the fact that the device provides the time derivative of the input signal's complex envelope when this signal is centered at the device's resonance frequency, i.e. when $\Delta\omega=0$ [39–44], see Eq. (1) below. This time-derivative relationship is fundamental to our derivation of the instantaneous-frequency recovery equation below.

Given that only a linear process is involved, the signal at the differentiator output is spectrally centered at the same carrier frequency, ω_0. We define the time-domain complex envelope of this output signal as $y(t)$ and its corresponding field spectrum as $Y(\omega)$. As for any linear time-invariant process, the field spectrum of the signal at the differentiator output is given by the product of the input field spectrum and the spectral transfer function of the differentiator, i.e. $Y(\omega)=X(\omega)\cdot D(\omega)=A\omega X(\omega)+A\Delta\omega X(\omega)$. From basic Fourier theory [45], it can be inferred that the corresponding time-domain waveform, $y(t)$, consists of two terms: the first term is proportional to the time derivative of the input complex envelope whereas the second term is directly proportional to this input envelope,

$$\begin{aligned} y(t) &= -jA\frac{\partial x(t)}{\partial t} + A\Delta\omega x(t) \\ &= A\exp(j\phi(t))\left\{[\Delta\omega|x(t)| + |x(t)|\omega_{inst}(t)] - j\frac{\partial|x(t)|}{\partial t}\right\} \end{aligned} \tag{1}$$

where $\omega_{inst}(t)=\dfrac{\partial\phi(t)}{\partial t}$ is the instantaneous frequency function of the signal under test. Notice that From Eq. (1), the temporal intensity profile of the signal at the differentiator output is:

$$|y(t)|^2 = A^2\left\{\left[\frac{\partial|x(t)|}{\partial t}\right]^2 + |x(t)|^2[\omega_{inst}(t)+\Delta\omega]^2\right\}. \tag{2}$$

If the frequency shift $\Delta\omega$ is sufficiently large so that it satisfies $\Delta\omega>|\omega_{inst}(t)|$ along the entire time duration of the signal under test, then

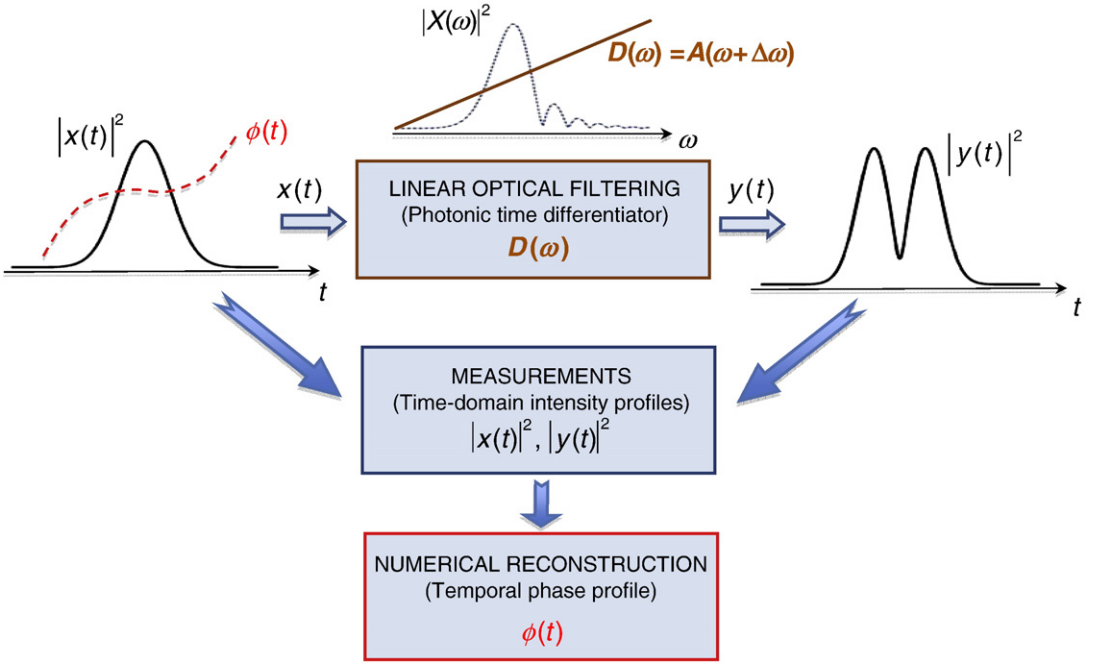

Fig. 1. Schematic of the concept for time-domain phase reconstruction based on optical ultrafast differentiation (PROUD).

the term $[\omega_{inst}(t)+\Delta\omega]$ in Eq. (2) is always positive and the instantaneous-frequency profile of the input signal can be *unambiguously* recovered from the measured temporal intensity profiles of the input signal, $|x(t)|^2$, and of the signal at the differentiator output, $|y(t)|^2$, using the following direct equation [33]:

$$\omega_{inst}(t) = \frac{\partial\phi(t)}{\partial t} = +s(t)-\Delta\omega \tag{3.a}$$

$$s(t) = \sqrt{\left(\frac{1}{|x(t)|^2}\right)\cdot\left(\left[\frac{|y(t)|}{A}\right]^2-\left[\frac{\partial|x(t)|}{\partial t}\right]^2\right)}. \tag{3.b}$$

The pulse temporal phase profile can be obtained by cumulative numerical integration of the recovered instantaneous frequency, except for an undetermined phase constant ϕ_0, i.e. $\phi(t)=\int_{-\infty}^{t}d\tau\omega_{inst}(\tau)+\phi_0$.

The above given condition $\Delta\omega>|\omega_{inst}(t)|$ simply implies that the frequency shifting $\Delta\omega$ has to be large enough to ensure that the *full* spectral content of the input signal is located at the high frequency side of the differentiator's resonance. Said other way, the lowest optical frequency of the input signal spectral support must be higher than the differentiator's resonance frequency. The same method can be applied when the full spectral bandwidth of the input signal is located at the low frequency side of the differentiator's resonance (i.e. when the highest optical frequency of the input signal is lower than the differentiator's resonance frequency). In this case, the spectral transfer function of the differentiator can be expressed as $D(\omega)=A(\omega-\Delta\omega)$, with $\Delta\omega$ being a positive number satisfying the above condition, and the resulting instantaneous-frequency recovery equation is:

$$\omega_{inst}(t) = -s(t) + \Delta\omega \tag{4}$$

where the function $s(t)$ is defined by Eq. (3.b).

2.2. Performance trade-offs of time-domain PROUD

As detailed in the introduction, a photonic differentiator can be practically implemented using a variety of technologies [39–44]. Photonic differentiators with wavelength bandwidths larger than 20 nm (~2.5 THz for signals spectrally centered around 1.5 μm) have been experimentally demonstrated and these devices can still be optimized to achieve even larger operation bandwidths [17]. Thus, in practice, the measurement bandwidth offered by time-domain PROUD does not appear to be fundamentally limited by the photonic differentiator technologies. In contrast, the ultimate constraints of a PROUD setup, in terms of spectral bandwidth and time duration of the signals that can be accurately characterized, are mainly imposed by the available instrumentation for measuring time-domain intensity profiles.

Time-domain PROUD is ideally suited for the characterization of low-power optical waveforms with full-width frequency bandwidths narrower than ~50 GHz. This corresponds to time features at least longer than ~10–20 ps. The time-domain intensity profiles of these waveforms and their linearly filtered counterparts can be accurately captured using a conventional high-speed photo-detector connected to a fast electronic sampling oscilloscope. Standard linear or non-linear optical pulse characterization methods are usually suitable for shorter optical waveforms, from the femtosecond to the picosecond range, and they cannot be easily extended for measurements over temporal durations exceeding a few tens of picoseconds [6]. Thus, time-domain PROUD represents a very simple and practical alternative for the complex-field characterization of narrow-band and/or long duration optical signals. Optical waveforms with bandwidths down to the sub-GHz range have been successfully characterized using this technique [33,36]. Moreover, even when the optical frequency bandwidth of the signal under test exceeds the photo-detection bandwidth, it is still possible to use the PROUD setup for accurate signal characterization as long as the radio-frequency (RF) spectra of the optical signal under test and its time derivative (i.e. spectra of their respective time-domain intensity profiles) are within the photo-detection bandwidth [33]. This is for instance the case when the signal under test exhibits a sufficiently large, predominantly quadratic phase variation (linear chirp) along its time-domain profile [33,35], see example in Section 2.3. This property can be exploited to extend the PROUD capabilities for optical pulse characterization down to the picosecond regime using a well-characterized first-order dispersive medium acting as a linear temporal stretcher over the original ultra-short pulse [35]. We have experimentally demonstrated accurate full characterization of picosecond pulses ranging from ~4 to ~20 ps with both continuous and discrete temporal phase profiles using this simple strategy [35].

A very important parameter to evaluate the performance of a phase reconstruction method is the phase sensitivity or minimum phase variation that can be accurately measured with the method. This parameter is in fact tightly related with the power sensitivity of the technique, which can be defined as the minimum pulse (average or peak) power that is necessary for phase reconstruction with a prescribed accuracy. The reader is addressed to Ref. [35] for a detailed study of the influence of the main design specifications in a PROUD system on the phase and power sensitivities provided by the measurement setup. Phase sensitivities enabling the accurate characterization of the group-velocity dispersion equivalent to standard single-mode fiber (SMF) sections as short as ~20 m have been demonstrated for Gaussian-like pulses extending over a full-width-at-half-maximum (FWHM) bandwidth of ~2 nm, temporally stretched by linear propagation through a 1 km-long SMF and with average powers well in the sub-milliwatt range.

Briefly, in time-domain PROUD, the phase sensitivity is improved as the signal-to-noise ratio (SNR) of the measured temporal intensity waveforms is increased. This implies that the phase sensitivity can be improved by increasing the average and/or peak powers of the signal under test and of the signal at the output of the photonic differentiator. The pulse energy at the photonic differentiator output increases with the slope magnitude ($|A|$) of the linear amplitude spectral response of the photonic differentiator: As a result, the sensitivity of the setup can be increased by use of a photonic differentiator with steeper linear spectral amplitude. The noise of the time-resolved intensity detection instrument directly affects the SNR in the measured patterns and consequently, it has a very important influence on the system sensitivity. Typically, the measurement SNR deteriorates as the spectral bandwidth of the intensity detection platform is increased. Thus, as a general design rule, a time-resolved intensity detection system with the lowest possible bandwidth should be used; the bandwidth should still be sufficient to accurately capture the time-domain intensity waveforms to be measured. An important consideration to keep in mind in a basic PROUD platform is that a large SNR in the measured time-domain intensity waveforms is usually necessary. This is in part due to the fact that the numerical instantaneous-frequency reconstruction procedure requires calculation of the derivative of the measured signal's time-domain amplitude profile (see Eq. (3.b)), making the procedure very sensitive to the presence of high-frequency noise in this measured waveform. As a result, a large averaging of the measured intensity waveform profiles is typically required [33,35]. In most cases, this requirement prevents application of the basic PROUD platform for single-shot optical signal characterization. Moreover, a numerical filtering procedure aimed to reduce the presence of high-frequency noise terms is also usually applied on the measured waveforms to increase the accuracy of the phase reconstruction process. Section 4 describes an advanced strategy, referred to as 'balanced' PROUD [36], enabling single-shot and real-time measurement capabilities.

Finally, we also note that precise temporal synchronization between the two measured time-domain waveforms is necessary to ensure phase reconstruction accuracy. The required level of synchronization depends inversely on the optical bandwidth of the signals under test: A

broader signal bandwidth implies a stricter tolerance on the time synchronization between the two measured waveforms. To give a reference, a time-delay accuracy of ~1 ps would translate into a maximum group-delay error of ~0.25% over a 2-nm signal spectral bandwidth (FWHM) [35] (defined as the maximum deviation between the measured and expected group-delay values within the measurement frequency bandwidth relative to the total group-delay range variation along this bandwidth). A simple and practical strategy for timing calibration of an experimental PROUD platform is described below in Section 2.3.

2.3. Experimental example of time-domain PROUD

Fig. 2 is a schematic of the experimental setup used in the demonstration revisited here [33]. The source of the seeding optical pulses was a passively mode-locked wavelength-tunable fiber laser (Pritel Inc.) operating at a repetition rate of 20 MHz. This source generated nearly transform-limited Gaussian-like optical pulses with a ~3 nm FWHM bandwidth (centered at ~1549 nm). The seeding pulse was filtered by an in-house tunable narrow band-pass filter (filtered down to a FWHM bandwidth of ~1.5 nm, centered at around 1553 nm, in the example reported here) and different phase profiles were imposed by linear and nonlinear propagation through optical fibers under different conditions. The pulses under test were amplified using an erbium-doped fiber amplifier. Typical average power of the pulses at the input of the PROUD system was measured to be ~615 μW. The optical differentiator was implemented using a single 55-mm long uniform LPFG operating in full-coupling condition (resonance dip of 40 dB, centered at 1551 nm) [40]. The amplitude coefficient of the used differentiator (typical value: $A = 0.304\ \mathrm{THz}^{-1}$) was directly determined by comparing the measured spectra of the input and differentiated pulses in our experiments, see Inset in Fig. 3(b). Notice that this estimate of the differentiator's amplitude coefficient A, to be used in the phase-recovery process, already includes any additional constant attenuation in the differentiator optical path relative to the signal optical path. The wavelength shifting between the input pulse and the optical differentiator was fixed to be around 2 nm ($\Delta\omega \approx 2\pi \times 250$ GHz), which ensured that the above-stated condition was always satisfied, $\Delta\omega > \max\{|\omega_{inst}(t)|\} \sim 2\pi \times 125$ GHz. The intensity profiles of both the input pulse under test $|x(t)|^2$ and the pulse after differentiation $|y(t)|^2$ were measured using a high-speed photodetector with a 3-dB bandwidth of 8 GHz attached to a 70-GHz sampling oscilloscope. In practice, it is important to ensure that the two measured intensity profiles are well synchronized. In our experiments, the time delay between the two measurement arms was first precisely calibrated by recording the spectral interference pattern with an 8-nm (full width) reference optical pulse. In particular, a free-space delay line was tuned to set a 1.08 ps delay (as determined by the spectral period of the recorded interferogram), which was subsequently compensated for in the numerical phase recovery process. While this precision level was sufficient for the cases evaluated in our testing experiments, the time synchronization should be set with a higher precision for phase reconstruction of optical pulses with shorter time features. For this purpose, a spectrally broader reference pulse should be used in the described interferometry strategy.

In the experiment reviewed here, PROUD was tested for retrieving a temporal phase profile comprising a continuous quadratic phase profile and a nearly discrete π phase shift. This discrete phase shift was induced from self-phase modulation (SPM) by propagation through a long section of dispersion-decreasing highly-nonlinear optical fiber. The broadened spectrum was band-pass filtered over a 1.5-nm FWHM bandwidth that comprised the SPM-induced π phase shift. The filtered pulse was then temporally stretched by linear reflection in a 10-m long linearly chirped fiber Bragg grating with a group-velocity dispersion of +1981 ps/nm. Fig. 3 (solid curves) shows the measured intensity profile and the recovered phase profile of the temporal waveform under test together with the numerically simulated curves (dashed curves). The measured quadratic phase profile agreed very well with the numerical estimations and the expected (equivalent) π phase shift at the pulse center was also accurately recovered.

3. Spectral-domain PROUD for (sub-)picosecond optical pulse measurements

3.1. Operation principle of spectral-domain PROUD

As illustrated in Fig. 4, spectral-domain PROUD [34] can be interpreted as the frequency-domain counterpart of time-domain PROUD (Section 2). The method is thus based on differentiation of the field spectrum, instead of temporal differentiation, and allows the precise numerical reconstruction of the spectral phase profile, $\Phi(\omega)$, of the signal under test, $X(\omega)$, from a set of two measured energy spectra (including the signal spectrum) using a direct and unambiguous algorithm. Full information on the complex field profile of the signal under test is obtained once both the spectral phase profile and signal energy spectrum are known. By relying on spectrally-resolved intensity measurements, one can overcome the bandwidth limitations imposed by the need for time-resolved intensity measurements in time-domain PROUD. Spectral-domain PROUD is thus ideally suited for full characterization of optical pulse waveforms with time features in the picosecond and sub-picosecond range. Spectral-domain differentiation can be easily implemented by time modulation of the optical signal with a linear amplitude waveform, see Fig. 4. This modulation process could be practically implemented using a variety of well-known alternatives for optical intensity modulation. In order to implement a fully linear measurement process, EO intensity modulation of the signal under analysis has been proposed [34]. This results in a simple and practical fiber-optics implementation.

Let us consider that the input optical signal under test, with complex envelope $x(t)$, is temporally modulated by a (positive) linear amplitude waveform, $d(t) = at + C$, where a (modulation slope) and

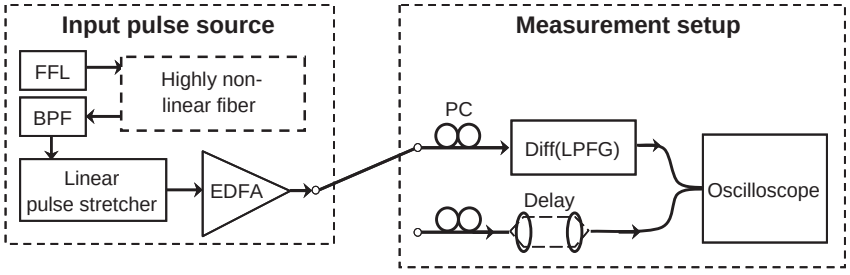

Fig. 2. Experimental setup used for our proof-of-concept demonstrations. FFL, femtosecond fiber laser; Diff (LPFG), long-period fiber grating differentiator; BPF, bandpass filter; EDFA, amplifier; PC, polarization controller.

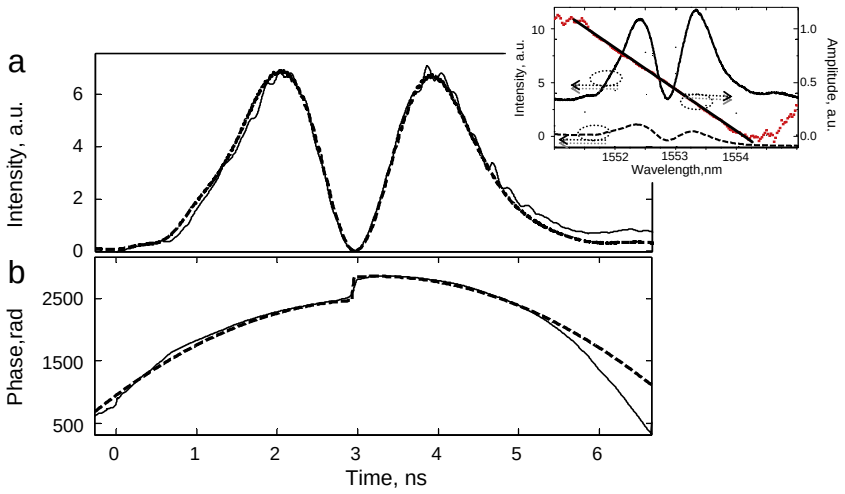

Fig. 3. Experimentally recovered (solid curves) and numerically simulated (dashed curves) amplitude (a) and phase (b) temporal profiles of the optical waveform under test. Inset: Measured intensity spectra of the signal under test (solid curve), and of the signal at the differentiator output (dotted curve). The plot also shows the calculated amplitude spectral transfer function of the optical differentiator (red squares) together with its linear curve fitting (black curve).

C (DC background) are positive real-valued parameters. The temporal complex envelope of the output signal from this modulation process is $y(t) = x(t) \cdot d(t) = at\ x(t) + Cx(t)$. Following a similar Fourier analysis to that of time-domain PROUD, it can be easily shown that the spectral energy density of the signal at the modulator output is given by the following expression:

$$|Y(\omega)|^2 = a^2\left\{\left[\frac{\partial|X(\omega)|}{\partial\omega}\right]^2 + |X(\omega)|^2\left[\tau_g(\omega) + \frac{C}{a}\right]^2\right\} \tag{5}$$

where $\tau_g(\omega) = -\dfrac{\partial\Phi(\omega)}{\partial\omega}$ is the group-delay of the signal under test. Thus, assuming that the inequality $(C/a) > |\tau_g(\omega)|$ holds over the entire spectral support of the signal under analysis, the signal's group-delay can be unambiguously calculated from measurements of the two energy spectra $|X(\omega)|^2$ and $|Y(\omega)|^2$ using the following analytic equation:

$$\tau_g(\omega) = -\frac{\partial\Phi(\omega)}{\partial\omega} = +S(\omega) - \left(\frac{C}{a}\right) \tag{6.a}$$

$$S(\omega) = \sqrt{\left(\frac{1}{|X(\omega)|^2}\right)\cdot\left(\left[\frac{|Y(\omega)|}{a}\right]^2 - \left[\frac{\partial|X(\omega)|}{\partial\omega}\right]^2\right)} \tag{6.b}$$

The input pulse spectral phase $\Phi(\omega)$ can be obtained from the result of Eq. (6) (except for a constant phase) by performing a cumulative integration of the recovered group delay. The time-domain complex

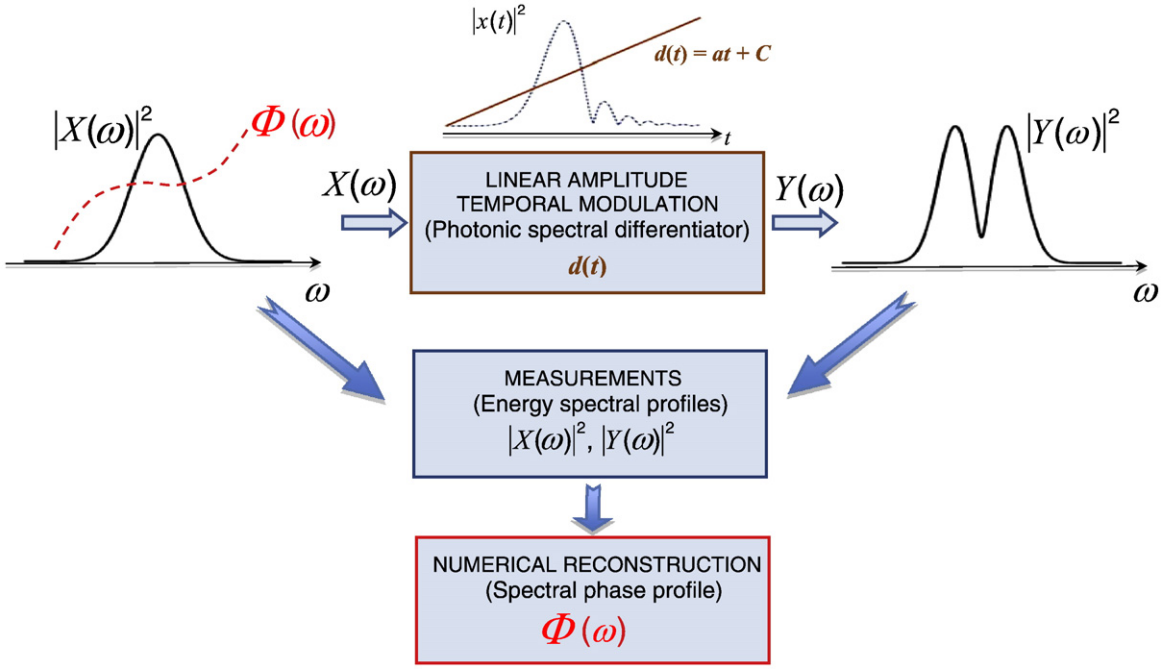

Fig. 4. Schematic of the concept for spectral-domain phase reconstruction based on optical ultrafast differentiation (PROUD). Notice that the time (t) and frequency (ω) variables are interchanged with respect to the illustration for time-domain PROUD in Fig. 1.

envelope of the pulse, $x(t)$, is directly given by the inverse Fourier transform of the obtained complex spectral field $X(\omega)=|X(\omega)|\exp[j\Phi(\omega)]$. The (positive) time amplitude modulation can also exhibit a negative slope, i.e. $d(t)=-at+C$, with a and C being both positive numbers. For an unambiguous phase reconstruction process, the same inequality as above should be satisfied. In this case, the following group-delay recovery equation should be used:

$$\tau_g(\omega) = -S(\omega) + \left(\frac{C}{a}\right) \tag{7}$$

with the function $S(\omega)$ defined in Eq. (6.b).

As mentioned above, a very convenient and practical way to implement the linear amplitude modulation on the optical pulse under analysis is to use EO intensity modulation with a sinusoidal RF signal. In the simplest case, one can use a Mach–Zehnder interferometer (MZI)-based EO intensity modulator operated at the transmission halfway between its maximum ($T=T_0$) and its minimum throughput ($T=0$). The transmission intensity function of this modulator is mathematically described by $T(V)=(T_0/2)\cdot(1+\sin[\pi V(t)/V_\pi])$, where $V(t)$ is the RF modulation signal and V_π is the half-wave voltage of the modulator. The EO modulator is driven by an electrical sinusoid $V(t)=V_0\sin(\Omega t)$, where V_0 is the modulation amplitude and Ω is the modulation angular frequency. To ensure that the optical pulse under test is carved by a linear amplitude modulation, the pulse must be synchronized with the modulation sinusoid at anyone of its cross-points with zero (e.g. around $t=0$) and the pulse duration must be much shorter than the modulation period, i.e. $\Delta t \ll 2\pi/\Omega$. In this case, the complex envelope of the optical pulse at the modulator output is

$$y(t) = \sqrt{T(V)}\cdot x(t) \approx \sqrt{T_0/2}\cdot[1 + B\Omega t]\cdot x(t) = at + C \tag{8}$$

where $B=\pi V_0/(2V_\pi)$, $a = B\Omega\sqrt{T_0/2}$, and $C = \sqrt{T_0/2}$. In deriving Eq. (8), we assume that the following additional inequality holds: $\Delta t \ll 2/(B\Omega)$. Notice that this latter inequality also ensures that the above stated condition for unambiguous phase recovery, i.e. $(C/a)>|\tau_g(\omega)|$, is necessarily satisfied ($|\tau_g(\omega)|<\Delta t/2$). Hence, for phase recovery using the described EO implementation, one needs to measure the energy spectra at the input and output of the modulator, $|X(\omega)|^2$, and $|Y(\omega)|^2$, respectively, and determine the parameters a and C for the employed setup; these latter parameters depend on the maximum modulator throughput, T_0, and the product $B\cdot\Omega$, all of which can be easily determined through simple measurements (see experimental example in Section 3.3). It is also important to note that the EO intensity modulator is assumed to introduce a negligible phase modulation on the incoming optical pulse. In practice, an MZI-based dual-drive (x-cut) EO modulator represents an ideal choice for our application since this modulator is specifically optimized to introduce a very low chirp.

3.2. Performance trade-offs of spectral-domain PROUD

Spectral-domain PROUD based on linear EO modulation is particularly well adapted to the characterization of picosecond and sub-picosecond pulses [34]. On the one hand, the time duration of the signal under test must be kept much smaller than the time period of the electrical modulation sinusoid. Similarly to time-domain PROUD, a high time modulation slope, $a = B\Omega\sqrt{T_0/2}$, is desired to improve the phase and intensity sensitivities of the measurement platform. This requires the use of high modulation frequencies, namely in the GHz range, which constraints the maximum time width of the optical pulse waveforms that can be accurately characterized with an EO spectral-domain PROUD system to a few tens of picoseconds. On the other hand, the characterization of a shorter pulse requires the use of a linear time modulation function with a higher slope. We estimate that pulses as short as 100 fs could be accurately characterized using a modulation frequency of 40 GHz, considering realistic parameters in the EO modulation process.

Generally speaking, the sensitivity of spectral-domain PROUD is exposed to equivalent design constraints to those of its time-domain counterpart (see Section 2.2). Given that an EO-based PROUD system is entirely linear, picosecond optical pulses with average intensities as low as a few microwatts can be accurately characterized using this approach [34]. It is particularly important to mention that the two required spectral energy spectra must be measured with a very high SNR to ensure an accurate group-delay (and phase) reconstruction using Eq. (6) or Eq. (7). The necessary integration time to capture these energy spectra with the required SNR, combined with the fact that two different spectra need to be measured, makes it very challenging to achieve the target pulse characterization process in a single shot and/or in real time. An advanced scheme, based upon the concept of 'balanced' spectral-domain differentiation, has been recently proposed and demonstrated to overcome these difficulties [38], enabling single-shot and real-time full characterization of picosecond and sub-picosecond pulse waveforms with tens of microwatts average optical powers. This scheme is reviewed in further detail in Section 4 below.

3.3. Experimental example of spectral-domain PROUD

As proof-of-concept experiments (schematic shown in Fig. 5), we tested picosecond pulses with well-characterized spectral phase profiles, which were induced by linear dispersion through 50–700 m long sections of single-mode fiber (SMF). In the set of experiments revisited here [34], a transform-limited 1.6-ps (FWHM) pulse (FWHM bandwidth ~1.53 nm), generated from a passively mode-locked fiber laser (Pritel Inc.) operating at 16.7 MHz repetition rate and at an optical wavelength of ~1551.5 nm, was used as the seeding input pulse. A portion (~10%) of the input pulse power was tapped using a fiber coupler and was used for generating a self-referenced RF sinusoidal modulation signal [46]. This RF generation technique utilizes frequency-to-time conversion [47–49] of a spectral pulse interference to generate a precisely time-synchronized optical modulation that is converted into the desired RF modulation signal through an amplified differential receiver. Precise time synchronization between the RF sinusoidal modulation signal and the input pulse was achieved by either simultaneously or consecutively monitoring the intensity modulation of CW laser light and the non-modulated input pulse train using a sampling oscilloscope. An example of the synchronized modulation at 2.4 GHz is shown in Fig. 6 (solid line), where it is observed that the linear part of the modulation sinusoid is located around the center of the input pulse (Fig. 6, dashed line). The coefficient $B\cdot\Omega$ was determined by fitting the modulation curve after intensity normalization ($T_0=1$) with a first-order polynomial (Fig. 6, dotted line), i.e. $\sqrt{I(t)}\rightarrow(1+B\Omega t)$. In our experiments, the value of the linear coefficient $B\cdot\Omega$ was between 5 and 7 [ns^{-1}]. The inverse of this value is much larger than the time width of any of the tested pulses, which ensures that (i) the time modulation process can be well approximated by a linear-amplitude function, and (ii) the above stated

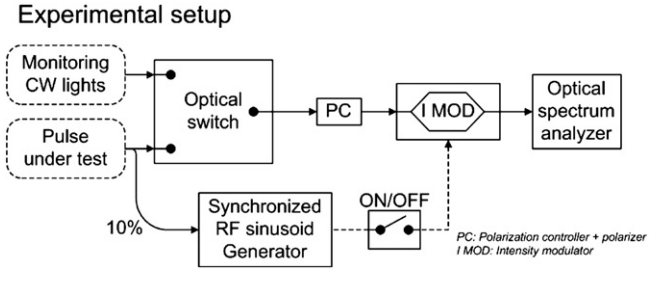

Fig. 5. Experimental setup of the proposed spectral-domain PROUD implementation.

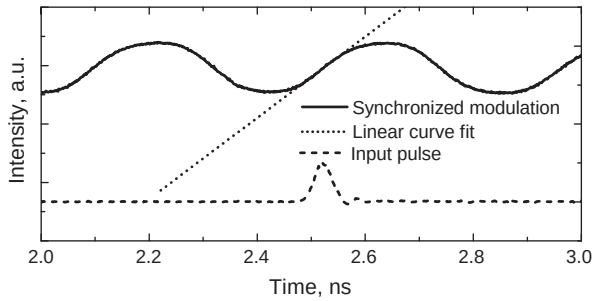

Fig. 6. Input pulse average optical intensity (dashed line) and temporal profile of the synchronized intensity modulation signal (solid line) both measured with a sampling oscilloscope. A linear curve fit of the modulation signal for determining the time modulation coefficient $B \cdot \Omega$ is also shown (dotted line).

condition for unambiguous phase recovery using Eq. (6) or Eq. (7) is satisfied. The input and the differentiated pulse spectra were acquired using an optical spectrum analyzer, OSA by sequentially turning on and off the RF driving signal in the modulator. The reconstructed spectral phases for the 100, 300, and 700 m propagation experiments are shown in Fig. 7(a) (solid lines), where the input average power before the modulator was 147 μW. Each of the recovered phase profiles matches very closely with the expected quadratic spectral phase curve over the entire input pulse spectrum. The recovered spectral phase profile for the 700 m propagation experiment using a lower input pulse power (17 μW) is also shown with hollow circles.

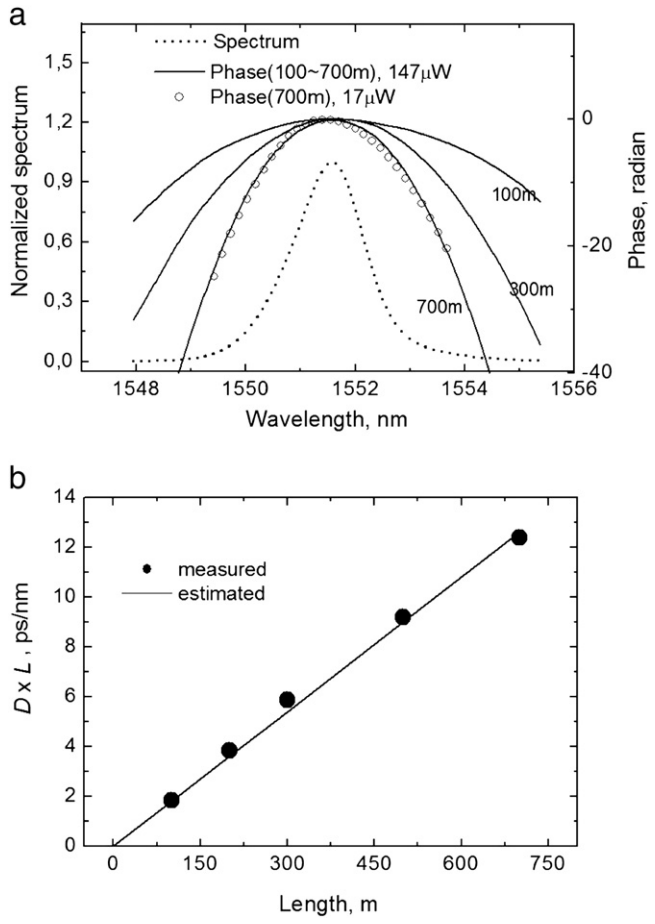

Fig. 7. (a) Measured energy spectrum (dotted line) and reconstructed phase profiles (solid lines) of dispersed pulses from a passively mode-locked fiber laser for different SMF lengths. Circles show the phase measured at a lower average power (17 μW). (b) Dispersion-length products (solid circles) determined from the reconstructed phase profiles in (a) and estimated curve of the SMF dispersion (solid line).

The accuracy of the reconstructed phase profiles was confirmed by calculating the dispersion-length (DL) product using a second-order polynomial fitting of the recovered phase curves. The corresponding dispersion-length values and a curve plotted considering the typical dispersion value of the SMF (18 [ps/(km·nm)] at 1550 nm wavelength) are shown in Fig. 7(b). For each of the tested waveforms, the amplitude and phase temporal profiles can be recovered by Fourier transformation of the reconstructed complex field spectrum.

It is worth noting that the phase reconstruction accuracy and power sensitivity in the spectral-domain PROUD experiment described here was limited by the timing jitter error (≤4.7 ps) of the generated RF sinusoids [46]. Significantly improved phase accuracy and power sensitivity were achieved in the characterization of optical pulses generated from an active-mode locking source, i.e. with GHz pulse repetition rates, by using the RF driving signal of the laser source for modulation in the spectral-domain differentiation scheme [34].

4. Balanced PROUD: single-shot and real-time optical phase reconstruction

4.1. Balanced PROUD: operation principle and performance trade-offs

4.1.1. Balanced time-domain PROUD

The numerical phase recovery algorithm in time-domain PROUD involves the calculation of the time derivative of the time-resolved input intensity, see Eq. (3). This numerical procedure is very sensitive to the presence of noise in the measured waveform, thus requiring a large averaging in the intensity detection process. An advanced extension of PROUD, referred to as 'balanced' PROUD [36], has been proposed and demonstrated to overcome this main difficulty of the original technique. In this scheme, there is no need for calculation of the numerical derivative of the measured signal's time-resolved intensity waveform to obtain the target instantaneous frequency profile. This fact combined with the noise suppression characteristics intrinsic to a balanced measurement method allows us to avoid the previously required time-averaged acquisition of the intensity waveforms. In this way, balanced PROUD can be used for single-shot detection of the instantaneous frequency chirp of a non-periodic (e.g. purely random) optical signal using a real-time digitizer.

A schematic of the balanced time-domain PROUD concept is shown in Fig. 8. The signal under analysis, with temporal complex envelope $x(t)$, is launched at the input of a 'balanced' frequency-shifted photonic temporal differentiator. This 'balanced' differentiator consists of two frequency discriminators with their respective linear-amplitude spectral transfer functions having (i) an identical slope magnitude and (ii) an identical frequency shift but with opposite sign (with respect to the signal's carrier frequency). Mathematically, the base-band spectral transfer functions of the two filters in the 'balanced' differentiator can be expressed as $D_+(\omega) = A(\omega + \Delta\omega)$ and $D_-(\omega) = -A(\omega - \Delta\omega)$, respectively, where we recall that $\Delta\omega$ is a positive number. In the notation used here, the spectral amplitude slopes of the two filters have been written down with an opposite sign. However, in general, one only needs to ensure that the magnitudes of the spectral amplitude slopes of the two filters are identical, regardless of their respective signs. What is important for balanced differentiation is that the two filters have the same frequency shift but with an opposite sign. The filter with $D_+(\omega)$ will be referred to as a 'positive-slope' differentiator whereas the filter with $D_-(\omega)$ will be referred to as a 'negative-slope' differentiator. Following a similar analysis to that in Section 2.1, it can be shown that the time-domain intensity profiles of the signals at the output of each of these optical filters ($y_+(t)$ and $y_-(t)$, respectively) are given by:

$$|y_\pm(t)|^2 = A^2 \left\{ \left[\frac{\partial |x(t)|}{\partial t} \right]^2 + |x(t)|^2 [\omega_{inst}(t) \pm \Delta\omega]^2 \right\}. \quad (9)$$

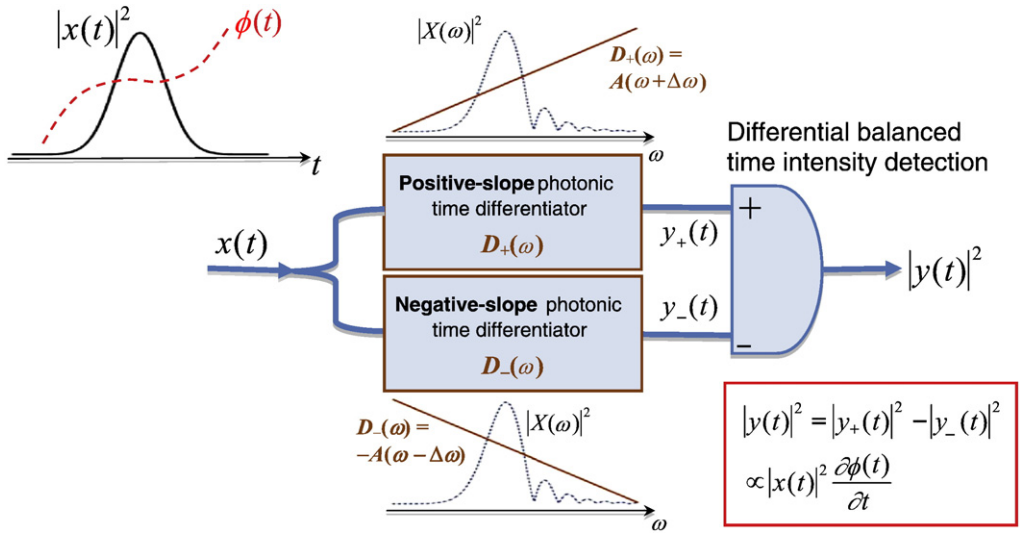

Fig. 8. Schematic illustration of the concept of balanced PROUD for single-shot and real-time optical signal characterization (time-domain implementation shown in the figure).

Differential (balanced) time-resolved intensity detection is used after the 'balanced' optical differentiator. This allows us to eliminate the common terms of the two intensity waveforms in Eq. (9), which include the temporal derivative of the input signal amplitude and random intensity noise terms (not written down explicitly in Eq. (9)). The measured intensity signal at the output of the differential intensity detection stage is thus given by [36]:

$$|y(t)|^2 = |y_+(t)|^2 - |y_-(t)|^2 = 4A^2\Delta\omega|x(t)|^2\omega_{inst}(t). \quad (10)$$

The input signal intensity, $|x(t)|^2$, can be directly measured using a standard time-resolved intensity measurement. In this way, the target instantaneous frequency profile, $\omega_{inst}(t)$, can be directly obtained from the measured temporal intensity at the differential detector output; the corresponding phase response $\phi(t)$ can be recovered from the measured instantaneous frequency using numerical integration. Single-shot, real-time detection of the instantaneous frequency and temporal phase profiles can be obtained using a high-speed digitizer (or real-time scope). In the particular case of a phase-only signal ($|x(t)|^2 \equiv$ constant), the instantaneous frequency profile can be directly visualized in the digitizer, following a proper calibration of the intensity scale, without needing any additional numerical post-processing, see Eq. (10). It is also worth mentioning that if the input temporal phase variation is a constant (e.g. for intensity-only optical modulation), the intensity profile at the differential detector output, Eq. (10), should be zero. This feature is used in practice to pre-calibrate the 'balanced' differentiation process.

'Balanced' photonic differentiation can be practically realized in a very simple fashion by use of a standard two-arm (2×2) interferometer, e.g. a fiber-optics or integrated-waveguide MZI, see schematic in Fig. 9(a) [44], [36]. The spectral transfer function at any of the two outputs of the interferometer when the signal to be processed (filtered) is launched at any of its two inputs is proportional to a sinusoidal variation with a period (free-spectral-range, FSR) determined by the inverse of the relative delay between the two arms of the interferometer. As a result, this filter provides the linear spectral amplitude variation that is required for photonic temporal differentiation over a limited bandwidth, i.e. a fraction of the filter's FSR, around any of its destructive resonance frequencies (at which the filter's transfer function approaches zero). In addition, it is well known that the spectral transfer functions at the two outputs of a 2×2 MZI are π phase shifted with respect to each other. Thus, these two transfer functions directly provide the desired 'positive-slope' and 'negative-slope' differentiation characteristics. Any of the frequency cross-points of these two spectral amplitude transfer functions (e.g. frequencies ω_1 and ω_2 marked in the schematic spectral response shown in Fig. 9(a)) is the 'balance point', in which the signal to be tested should be spectrally centered, resulting in an amplitude coefficient (A) and frequency shift ($\Delta\omega$) identical in magnitude but with opposite sign for the two differentiation transfer functions.

The described differential time-resolved intensity detection scheme can be implemented in a very straightforward fashion using a conventional balanced photo-detector, namely two identical photo-detectors with their outputs connected to a differential electrical amplifier. Balanced photo-detectors with bandwidths up to a few tens of GHz are readily available; thus, the measurement bandwidth constraints of this approach are similar to those discussed above for the basic time-domain PROUD technique using standard photo-detection (Section 2.2). Balanced time-domain PROUD has proved ideally suited for characterization of the instantaneous-frequency profiles of GHz-bandwidth random telecommunication data stream signals [36]. Moreover, by exploiting the intrinsic periodicity of the spectral transfer function of the interferometer, multi-wavelength signals can be simultaneously characterized using a single optical filtering and detection platform (see Section 4.2) [37].

The implementation complexity of time-domain PROUD is similar to a Differential Phase Shift Keying (DPSK) demodulation system [9]. We reiterate that time-domain PROUD enables detection of arbitrary instantaneous-frequency variations, within its performance constraints, in contrast to a conventional DPSK demodulator, which is designed for differential phase detection of data signals with a predefined phase modulation format and bit rate.

4.1.2. Balanced spectral-domain PROUD

The 'balanced' differentiation concept for optical signal characterization can be also applied to improve the performance of spectral-domain PROUD [38]. It is relatively straightforward to outline the frequency-domain counterpart of the time-domain balanced PROUD concept. Briefly, the optical pulse under test should be temporally modulated in intensity by two linear amplitude temporal modulations, $d_+(t)$ and $d_-(t)$, both having an identical slope but with opposite sign, and the same DC background, mathematically $d_\pm(t) = \pm at + C$. These balanced temporal modulation operations can be practically implemented using a single EO intensity modulator driven by an electrical sinusoid, in which two replicas of the optical pulse under analysis are synchronized with the positive-slope and negative-slope linear portions of the modulation sinusoid, respectively. The pulse's group delay, enabling a recovery of the spectral

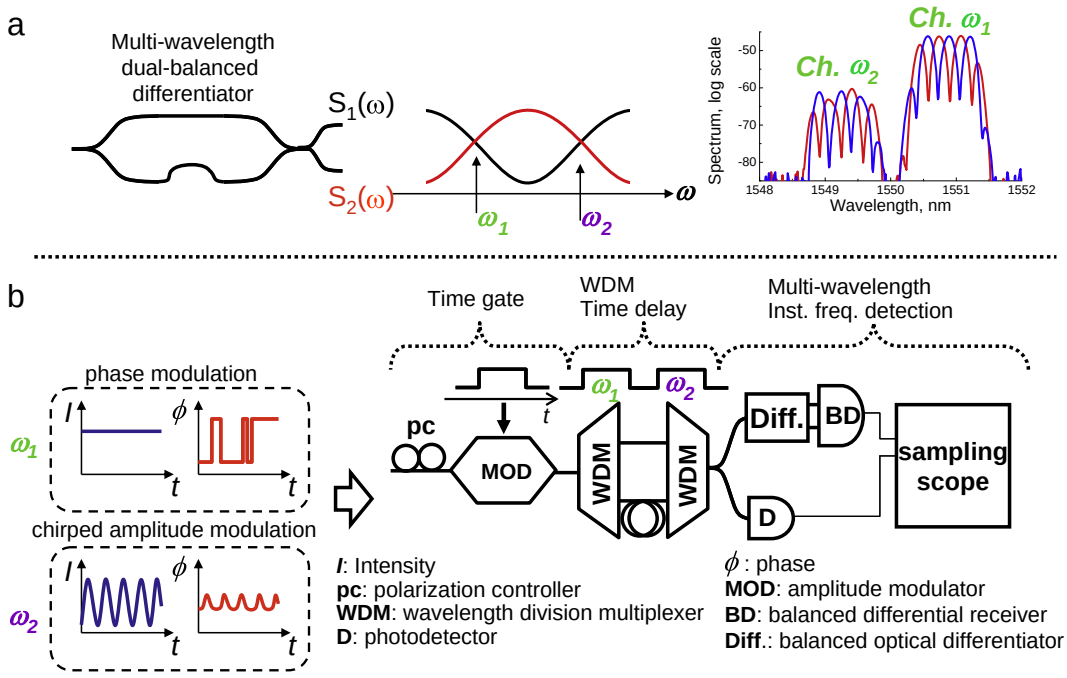

Fig. 9. (a) Principle of multi-wavelength balanced differentiation. (b) Experimental diagram for measuring the instantaneous frequencies of two wavelength channels (ω_1 an ω_2) based on the multi-wavelength balanced PROUD technique.

phase profile, can be directly obtained from the difference between the spectral energy densities at the outputs of the two modulation operations, namely

$$|Y(\omega)|^2 = |Y_+(\omega)|^2 - |Y_-(\omega)|^2 = 4aC|X(\omega)|^2\tau_g(\omega). \quad (11)$$

For group-delay reconstruction, the input pulse energy spectrum should be also measured. The advantages of the use of the balanced concept in spectral-domain PROUD over the basic single-modulation scheme are similar to those described above for the time-domain PROUD platform. Balanced spectral-domain PROUD offers a significantly improved SNR performance while avoiding the need to calculate a time derivative of the measured pulse spectral amplitude. These key improvements have enabled the extension of spectral-domain PROUD for single-shot and real-time full characterization of low-power (microwatt) optical pulses in the picosecond and sub-picosecond regimes [38], see more details in Section 4.3 below.

4.2. Experiments on time-domain balanced PROUD: single-shot and real-time phase reconstruction of multi-wavelength optical signals

As discussed in the previous Section 4.1, time-domain balanced PROUD can be implemented in a very simple fashion using a conventional 2×2 interferometer. One can take advantage of the spectrally periodic response of the interferometer to extend the capabilities of PROUD for simultaneous characterization of many multi-wavelength signals, such as those to be found in a WDM fiber-optic communication system. Using this simple strategy, we have demonstrated single-shot and real-time measurements of the instantaneous frequency and phase profiles of WDM signals in a simultaneous fashion using a single optical signal processing and photo-detection platform [37]. This method dramatically simplifies the detection process by avoiding the need for stable multi-wavelength (or wavelength-tunable) optical reference sources.

A schematic of the concept for multi-wavelength signal phase characterization is illustrated in Fig. 9(a), in which the spectral transfer functions corresponding to the two outputs of a 2×2 MZI are also shown. The dual balanced differentiation operation range can be found around each of the cross-point frequencies of the interferometer over a bandwidth given by a fraction of the FSR. Furthermore, since the respective spectral transfer functions repeat periodically along the optical spectrum with a period defined by the interferometer's FSR, the same dual-balanced differentiation process can be simultaneously applied over many wavelength channels for WDM signal analysis and characterization. The inset in Fig. 9(a) also shows an example of the spectrally periodic transfer function of the used fiber-optics MZI-based balanced differentiator with a relative length difference ~4.8 mm (corresponding to a 41-GHz FSR) at two different wavelength channels (ω_1 and ω_2), where both channels are multiplexed via a WDM filter with a 200-GHz channel spacing. This scheme provides a detectable instantaneous-frequency bandwidth exceeding 15 GHz.

To illustrate the measurement capabilities of our method, different modulation formats were employed in each of the tested wavelength channels. In particular, the optical signal centered at 1550.9 nm ($\omega_1 = 2\pi \times 193.4$ THz) was modulated in phase with a 3-Gbps PRBS (pseudo-random binary sequence with a total number of bits $= 2^{15} - 1$), whereas the optical signal centered at 1549.3 nm ($\omega_2 = 2\pi \times 193.6$ THz) was modulated in amplitude with a sinusoid at 1 GHz and subsequently amplified in a semiconductor optical amplifier (SOA) inducing additional frequency chirp due to the gain modulation. To give a reference on the power levels of the tested data streams, we measured a minimum average power of 260 μW for the amplitude modulated signal (before temporal gating). The two wavelength-multiplexed optical signals were combined through a WDM filter (not shown in the diagram). To be able to display the two characterized results in a single oscilloscope channel, the signals were first temporally gated over a time duration of ~42 ns using an EO intensity modulator and subsequently time delayed with respect to each other using a paired WDM filter system and a fiber delay line. The gated and delayed signals were differentiated in the balanced optical differentiator. The fiber interferometer arms were tightly fixed on a package to ensure the needed stability in the filter's spectral response during the measurement time. For increased stability, alternative solutions similar to those developed for DPSK demodulation

[9] could be employed. The two differentiated outputs were sent to a 23-GHz (3-dB bandwidth) balanced photoreceiver and sampled at 25 Giga-samples-per-second (GS/s) using a real-time oscilloscope with a 3-dB bandwidth of 8 GHz. The input signal intensity waveforms were detected and sampled through the other fiber-coupler output using a 2.8-GHz single-ended photodetector.

An example of a single-shot measurement is shown in Fig. 10 with calibrated instantaneous-frequency scales. Fig. 10(a) shows the directly acquired waveforms from the balanced differentiation output (brown color) and the original signal intensity (orange color) at 25 GS/s. The time-domain phase profiles of the modulated signals were also directly calculated from the measured instantaneous-frequency profiles using numerical cumulative integration. Fig. 10(b) and (c) show the direct acquisitions of the instantaneous-frequency profiles for the phase modulated (b) and the amplitude modulated (c) signals with properly calibrated scales. The numerically recovered phase profiles are shown in Fig. 10(d) and (e), respectively. In all cases, the recovered instantaneous-frequency and temporal phase profiles were in excellent agreement with the expected ones [37].

4.3. Experiments on spectral-domain balanced PROUD: single-shot and real-time characterization of (sub-)picosecond optical waveforms

As described in Section 4.1, for balanced spectral-domain differentiation, two linear-amplitude temporal modulations should be applied on the pulse under test. These two linear-amplitude modulations should exhibit the same slope but with opposite signs and the same DC background, mathematically $d_{\pm}(t) = \pm at + C$. These balanced temporal modulation operations can be practically implemented using a single EO intensity modulator driven by an electrical sinusoid, $V(t) = V_0 \sin(\Omega t)$, in which two replicas of the optical pulse under analysis are synchronized with the positive-slope and negative-slope linear portions of the modulation sinusoid, e.g. centered at $t = 0$ and $t = T/2 = \pi/\Omega$, respectively. The pulse time width should be sufficiently short to satisfy the same conditions as for the basic EO spectral-domain PROUD technique (see conditions in Section 3.1). In this case, the desired linear-amplitude time modulation functions are implemented with the following parameters: $a = B\Omega\sqrt{T_0/2}$, and $C = \sqrt{T_0/2}$. We recall that $B = \pi V_0/(2V_\pi)$ and T_0 is the maximum throughput of the intensity modulator, which is assumed to be biased at half this maximum throughput.

The group-delay profile of the pulse under test can be recovered from Eq. (11) using the set of parameters defined in the above paragraph. As discussed above, three energy spectra need to be measured, $|Y_+(\omega)|^2$, $|Y_-(\omega)|^2$, and $|X(\omega)|^2$. To achieve these measurements in a single-shot, we employ dispersion-induced frequency-to-time mapping, FTM (also referred to as real-time Fourier transformation [47–49]). Briefly, FTM is based on transferring the energy spectrum of an incoming time-limited optical waveform along the time axis using large group-velocity dispersion: Following a simple linear propagation of the optical waveform

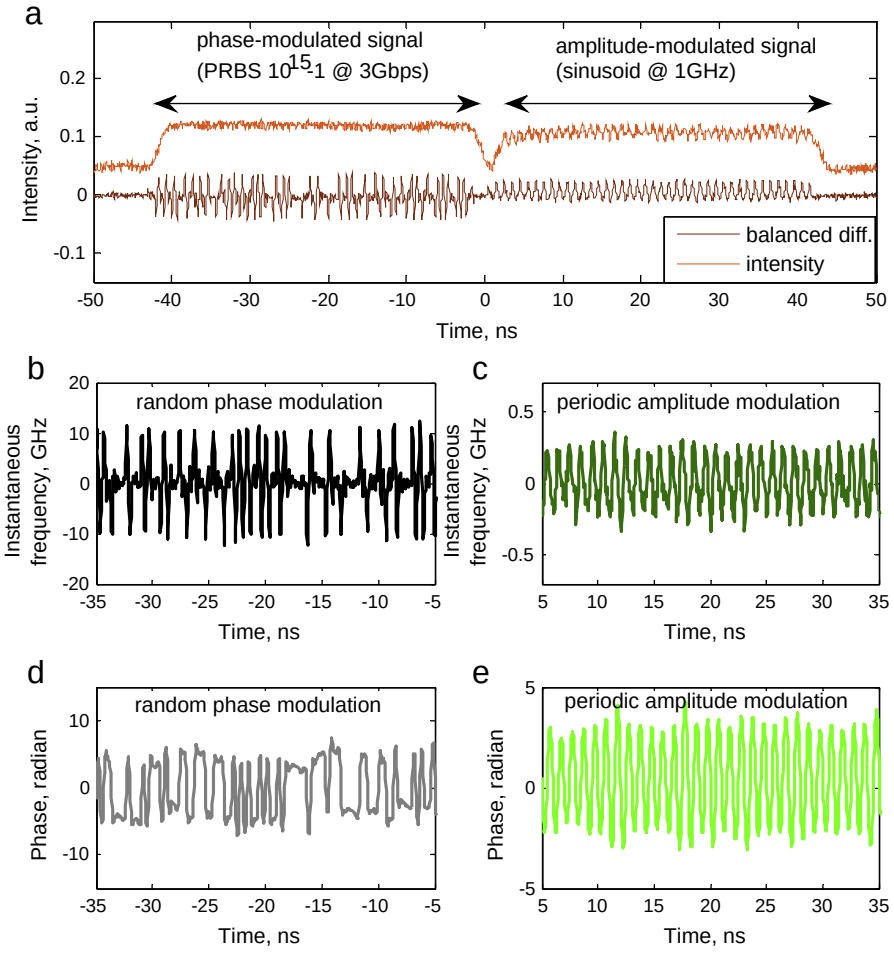

Fig. 10. Direct single-shot and real-time measurement of the instantaneous frequency (IF) and the phase profiles of two signals centered at two different wavelength channels (ω_1 and ω_2). (a) A full-scale view of the direct simultaneous acquisition of the IF profiles at two different wavelength channels. Direct simultaneous acquisition of the calibrated IF profiles at two different wavelength channels for (b) the phase modulation (signal at ω_1) and (c) the amplitude modulation (signal at ω_2). Recovered temporal phase profiles for the phase modulation (d) and the amplitude modulation (e), respectively.

under test through a dispersive medium (e.g. reflection in a linearly chirped fiber Bragg grating, LCFG, such as in our experiments), one obtain a time-domain intensity waveform at the system output that is proportional to the pulse energy spectrum. In our setup, the three pulse signals to be measured are first temporally interleaved and this is followed by dispersion-induced FTM via reflection in a LCFG. In this way, the energy spectra of the three pulse waveforms can be captured *consecutively* in a single-shot and in real-time by use of a high-speed photo-detector connected to a fast digitizer.

Real-time monitoring of an ultra-short optical pulse compression process in a highly-nonlinear fiber was conducted by single-shot measurements of the intensity and phase profiles of the pulses obtained at the fiber output [38]. A schematic of the experimental setup is shown in Fig. 11(a). A transform-limited ~2 ps (FWHM) pulse generated from a passively mode-locked fiber laser (Pritel Inc.) with a repetition rate of 5 MHz and at a wavelength of ~1551.7 nm, was used as the original pulse to be compressed. The original pulse was compressed down to the sub-picosecond regime (~0.92 ps, FWHM) by monotonically increasing the input pulse power. The pulse experienced spectral broadening induced by self-phase modulation (SPM) as it propagated through the fiber and was simultaneously compressed by the dispersion-decreasing feature along the fiber. Half of the input pulse power was tapped using a fiber coupler and polarized for proper modulation in a MZM (3 dB-bandwidth of 35 GHz) whereas the other half was used for generating a *self-referenced* RF sinusoidal modulation signal. In particular, a precisely synchronized RF sinusoidal wave-packet at 9.9 GHz was generated using the technique described in Ref. [46]. Fiber-optic time interleavers were applied both for the optical pulse under test and for the self-referenced RF source to prepare two time-delayed copies of the optical pulse and the RF modulation wave-packet. In this way, the two desired opposite-slope temporal modulation processes were achieved in the same MZM, as illustrated in Fig. 11(a). The time delay between the two pulse copies was fixed to 29.3 ns. A 10-m long LCFG (2 ns/nm, 42 nm bandwidth, Proximion Inc.) was used for the FTM, limiting the maximum spectral bandwidth for the pulse under test to ~15 nm, as restricted by the time delay fixed in the interleaver (to avoid temporal overlapping among consecutive temporally-stretched waveforms). Fig. 11(b) presents two consecutive replicas of the optical pulse under test and the corresponding time-synchronized modulating RF signal, showing how the two pulses undergo the desired opposite-slope linear modulations. A second interleaver was used to insert the original pulse under test after the two spectrally-differentiated waveforms, with the same inter-pulse delay of ~29.3 ns; in this way, the three corresponding spectra were consecutively mapped along the time axis after FTM by the LCFG. A 3-GHz single-ended photo-detector and a real-time oscilloscope (8 GHz bandwidth) were used for acquisition of the time-domain waveforms. The group-delay profile of the pulse under test was numerically recovered from the measured spectra, following a suitable time-to-frequency scaling according to the nominal group-delay slope of the LCFG, using Eq. (11). Fig. 12(a) and (b) show the spectral- and the time-domain intensity and phase profiles of the reconstructed output pulses for two different compression conditions, i.e. for input average powers of 32.5 μW and 185 μW, respectively.

5. Conclusions

This paper reviews recent work on a new group of linear, self-referenced techniques for fast optical signal characterization based on time-domain or frequency-domain photonic differentiation, namely PROUD methods. These techniques can be implemented in very simple and practical fiber-optics configurations using widely available optical fiber and RF components and measurement instruments. In addition, phase recovery is based on the use of a direct, non-iterative numerical algorithm. PROUD methods have proved suitable for full characterization of optical signals over a very broad range of time durations and spectral bandwidths, e.g. with time features ranging from the sub-picosecond to the nanosecond regime, and with average powers as low as a few microwatts. These stringent measurement specifications can be achieved in a single shot and in real time using balanced photonic differentiation schemes. PROUD methods are ideally suited for applications in the context of high-speed optical telecommunications and linear ultra-fast computing and information processing circuits. Extension of PROUD measurement techniques for their use over a broader range of pulse durations, frequency

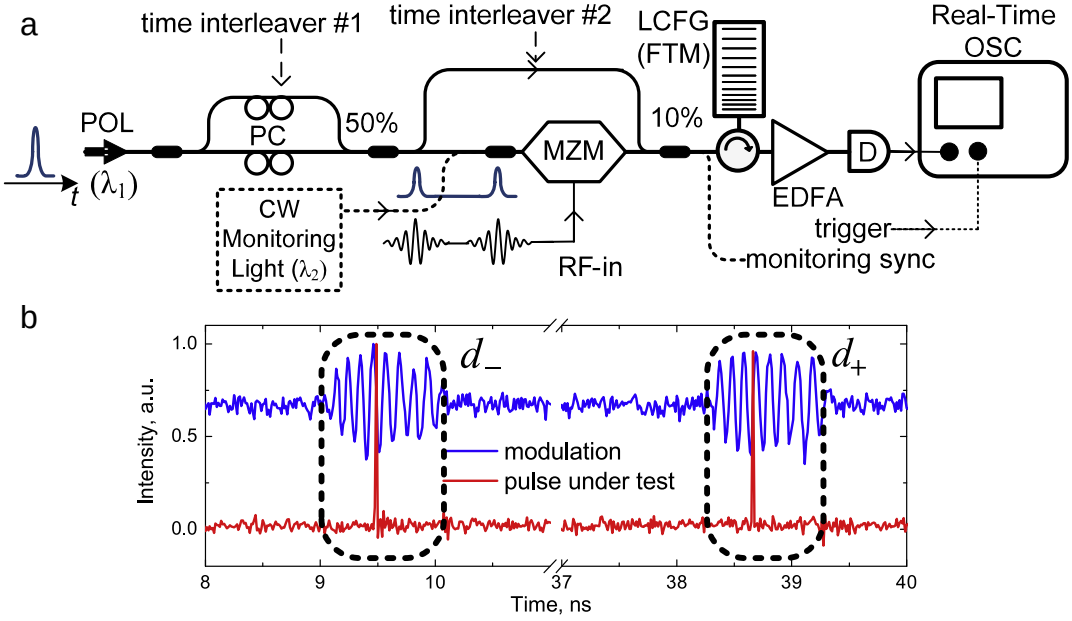

Fig. 11. (a) Schematic of proof-of-concept experimental setup for balanced spectral-domain PROUD. POL: polarizer. PC: polarization controller. MZM: electro-optic Mach–Zehnder modulator. LCFG: linearly chirped fiber Bragg grating. EDFA: erbium-doped fiber amplifier. Real Time-OSC: real-time oscilloscope. Monitoring sync: Signal used for monitoring the synchronization between the temporal modulation (λ_2) and the two time-delayed copies of the pulse under test (λ_1). (b) Synchronization of the two time-delayed copies of the pulse under test (red) and the RF modulation signal (blue).)

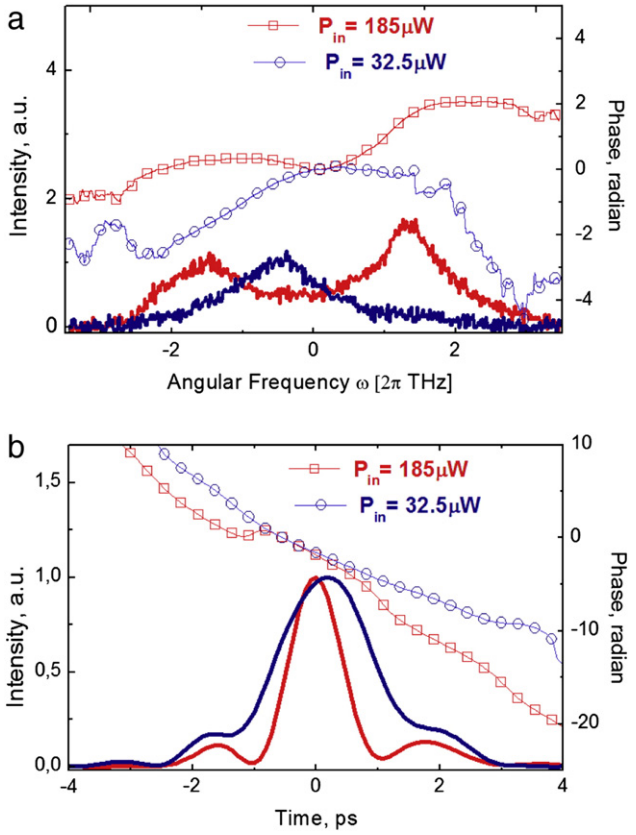

Fig. 12. Single-shot, real-time ultra-short pulse measurements by spectral-domain balanced PROUD: (a) Reconstructed spectral phase profiles of an optical pulse temporally compressed by a nonlinear fiber for two different input powers of 32.5 μW (circles) and 185 μW (squares). The spectrum profiles of the compressed pulses are also shown. (b) Reconstructed temporal intensity and phase profiles of the compressed pulses.

bandwidths and wavelength regions with increased sensitivities and improved capabilities can be anticipated.

Acknowledgements

We would like to express our deepest gratitude to many of our colleagues for insightful discussions and direct contributions on some of the topics presented here. We are particularly indebted to the following persons: Tae-Jung Ahn (Chosun University, South Korea), Mirco Scaffardi and Luca Potì (CNIT — Pisa, Italy), Antonio Malacarne (INRS-EMT), Radan Slavík (Univ. of Southampton, UK), Jianping Yao (Univ. of Ottawa, Canada), Greg Schinn (Exfo Inc., Canada), and Ignacio Esquivias (Universidad Politecnica de Madrid, Spain).

This work was supported in part by the Natural Sciences and Engineering Research Council (NSERC) through its Strategic Project Grants program.

References

[1] A.M. Weiner, Ultrafast Optics, John Wiley & Sons, Hoboken, NJ, 2009.
[2] C. Froehly, B. Colombeau, M. Vampouille, in: E. Wolf (Ed.), Progress in Optics XX, North-Holland, 1983, p. 63,, Chap. II.
[3] R. Trebino, Frequency-Resolved Optical Gating: The Measurement of Ultrashort Laser Pulses, Kluwer, Norwell, MA, 2004.
[4] C. Dorrer, I.A. Walmsley, EURASIP J. Appl. Signal Proc. 10 (2005) 1541.
[5] C. Dorrer, I. Kang, J. Opt. Soc. Am. B 25 (2008) A1.
[6] I.A. Walmsley, C. Dorrer, Adv. Opt. Photonics 1 (2009) 308.
[7] C. Dorrer, IEEE J. Sel. Top. Quantum Electron. 12 (2006) 843.
[8] G.P. Agrawal, Fiber-Optic Communication Systems, 3rd ed.Wiley Interscience, New-York, NY, 2002.
[9] A.H. Gnauck, P.J. Winzer, IEEE OSA J. Lightwave Technol. 23 (2005) 115.
[10] E. Ip, A.P.T. Lau, D.J.F. Barros, J.M. Kahn, Opt. Express 16 (2008) 753.
[11] N.K. Fontaine, R.P. Scott, L. Zhou, F. Soares, J.P. Heritage, S.J.B. Yoo, Nat. Photonics 4 (2010) 248.
[12] D.J. Kane, R. Trebino, Opt. Lett. 18 (1993) 823.
[13] C. Iaconis, I.A. Walmsley, Opt. Lett. 23 (1998) 792.
[14] L. Lepetit, G. Chériaux, M. Joffre, J. Opt. Soc. Am. B 12 (1995) 2467.
[15] V.R. Supradeepa, D.E. Leaird, A.M. Weiner, Opt. Express 17 (2009) 14434.
[16] N.K. Fontaine, R.P. Scott, J.P. Heritage, S.J.B. Yoo, Opt. Express 17 (2009) 12332.
[17] J. Azaña, IEEE Photonics J. 2 (2010) 359.
[18] C. Dorrer, I. Kang, Opt. Lett. 27 (2002) 1315.
[19] D. Reid, J. Harvey, IEEE Photon. Technol. Lett. 19 (2007) 535.
[20] C. Dorrer, I. Kang, Opt. Lett. 28 (2003) 477.
[21] J. Bromage, C. Dorrer, I.A. Begishev, N.G. Usechak, J.D. Zuegel, Opt. Lett. 31 (2006) 3523.
[22] P. Kockaert, J. Azaña, L.R. Chen, S. LaRochelle, IEEE Photon. Technol. Lett. 16 (2004) 1540.
[23] R.M. Fortenberry, W.V. Sorin, H. Lin, S.A. Newton, Conference on Optical Fiber Communication, 1997, p. 290.
[24] C. Dorrer, Opt. Lett. 29 (2004) 204.
[25] T.J. Ahn, Y. Park, J. Azaña, IEEE Photon. Technol. Lett. 20 (2008) 475.
[26] Y. Park, T.-J. Ahn, J. Azaña, Opt. Express 17 (2009) 1734.
[27] N.S. Bergano, Electron. Lett 24 (1988) 1296.
[28] R.A. Saunders, J.P. King, I. Hardcastle, Electron. Lett 30 (1994) 1336.
[29] C. Laverdière, A. Fekecs, M. Têtu, IEEE Photon. Technol. Lett. 15 (2003) 446.
[30] K. Sato, S. Kuwahara, Y. Miyamoto, IEEE OSA J. Lightwave Technol. 23 (2005) 3790.
[31] M. Matsuura, N. Iwatsu, K. Kitamura, N. Kishi, IEEE Photon. Technol. Lett. 20 (2008) 2001.
[32] I. Kang, C. Dorrer, Opt. Lett. 30 (2005) 1545.
[33] F. Li, Y. Park, J. Azaña, Opt. Lett. 32 (2007) 3364.
[34] J. Azaña, Y. Park, T.-J. Ahn, F. Li, Opt. Lett. 33 (2008) 437.
[35] F. Li, Y. Park, J. Azaña, IEEE OSA J. Lightwave Technol. 27 (2009) 4623.
[36] F. Li, Y. Park, J. Azaña, Opt. Lett. 34 (2009) 2742.
[37] Y. Park, M. Scaffardi, L. Potì, J. Azaña, Opt. Express 18 (2010) 6220.
[38] Y. Park, M. Scaffardi, A. Malacarne, L. Potì, J. Azaña, Opt. Lett. 35 (2010) 2502.
[39] N.Q. Ngo, S.F. Yu, S.C. Tjin, C.H. Kam, Opt. Commun. 230 (2004) 115.
[40] R. Slavík, Y. Park, M. Kulishov, R. Morandotti, J. Azaña, Opt. Express 14 (2006) 10699.
[41] L.-M. Rivas, K. Singh, A. Carballar, J. Azaña, IEEE Photon. Technol. Lett. 19 (2007) 1209.
[42] Y. Park, T.-J. Ahn, J. Azaña, Appl. Opt. 47 (2008) 417.
[43] F. Liu, T. Wang, L. Qiang, T. Ye, Z. Zhang, M. Qiu, Y. Su, Opt. Express 16 (2008) 15880.
[44] Y. Park, J. Azaña, R. Slavík, Opt. Lett. 32 (2007) 710.
[45] A.V. Oppenheim, A.S. Willsky, S.N. Nawab, S.H. Nawab, Signals and Systems, 2nd ed.Prentice Hall, Upper Saddle River, NJ, 1996.
[46] Y. Park, T.-J. Ahn, F. Li, J. Azaña, IEEE Photon. Technol. Lett. 20 (2008) 1115.
[47] Y.C. Tong, L.Y. Chan, H.K. Tsang, IEEE Photon. Technol. Lett. 33 (1997) 983.
[48] J. Azaña, M.A. Muriel, IEEE J. Quantum Electron. 36 (2000) 517.
[49] Y. Park, T.-J. Ahn, J.-C. Kieffer, J. Azaña, Opt. Express 15 (2007) 4597.